Allowable Received OTDR Light Power for In-Service Measurement in Lightwave SCM Systems

Fumihiko Yamamoto and Tsuneo Horiguchi, *Senior Member, IEEE, Member, OSA*

***Abstract*—To measure in-service optical transmission lines in optical video distribution systems using subcarrier multiplexing (SCM) techniques, we clarify how measurement light from an optical time domain reflectometer (OTDR) affects the signal transmission performance when the light enters an optical network unit (ONU). We describe the additional noises induced when OTDR light is injected into the ONU and analyze the relationship between received OTDR light power and carrier-to-noise ratio. Moreover, we use the analysis to provide a technique for estimating the allowable received light power in lightwave SCM systems and show the dominant factors determining this allowable power. Finally, by using the estimation technique, we clarify the required rejection ratio for a filter designed to prevent OTDR light from entering ONU's in wavelength division multiplexing systems.**

***Index Terms*—In-service testing, optical time domain reflectometer (OTDR), subcarrier multiplexing (SCM), wavelength-division multiplexing (WDM).**

I. Introduction

RECENTLY, optical video distribution systems using subcarrier multiplexing (SCM) techniques have been researched and developed in many organizations for high capacity optical access networks [1]–[5]. This is because lightwave SCM systems, employed in conjunction with passive optical splitters, can help us to build low-cost broadband networks, and they have great flexibility to respond to consumer demands for rapid increases in channel capacity since individual channels are independent. To make the systems compatible with existing equipment, amplitude-modulated vestigial sideband (AM-VSB) video signals are transmitted over optical fibers in the SCM systems [6]. When providing high quality service to customers in such analog fiber-optic systems, optical network units (ONU's) installed on customers' premises must receive optical signals with a high carrier-to-noise ratio (CNR). Therefore, the splice losses and reflectivities of optical connectors must be reduced in optical transmission lines [7], [8]. In other words, the service quality depends on the splice losses and reflectivity. This means that supervisory systems which test these lines are very important as regards maintaining service quality.

To provide effective preventive maintenance and the prompt location of faults in optical transmission lines, NTT has developed in-service measurement systems which can be applied to lightwave SCM systems [9]. Fig. 1 shows the configuration of the in-service measurement system proposed in [9]. A synchronous transfer mode (STM) signal with a wavelength in the 1.3-μm region and an SCM signal in the 1.5-μm region are multiplexed by wavelength division multiplexing (WDM) techniques, and these signals are sent to ONU's via optical transmission lines. In these WDM systems, the splice losses and reflectivities of optical connectors are measured with only one optical time domain reflectometer (OTDR) which is installed in a central office. A measurement light from the OTDR is launched into a tested line via an optical switch and an optical coupler. Since the service quality is degraded by injecting the OTDR light into the ONU, the light wavelength is set in the 1.6-μm band which is different from the STM and SCM signal wavelength regions and a short wavelength pass filter (SWPF) is inserted in front of the ONU to prevent the OTDR light from entering it. Therefore, we must estimate the required rejection ratio of the SWPF for in-service measurement, which means it is very important to clarify the allowable received power of the OTDR light at the ONU. Although the effect of the OTDR light on STM signal quality was studied in [10], it has yet to be reported in detail for lightwave SCM systems.

In this paper, we present a way of estimating the allowable received OTDR light power in lightwave SCM systems and describe the dominant factors for determining the power. Section II discusses theoretical estimates of additional noise caused within the SCM signal band when OTDR light enters an ONU. The features of the additional noise is also clarified in this section. In Section III, we measure the quantitative CNR degradation caused by the OTDR light injection for a 40-channel lightwave SCM system. We also calculate its value using the analysis of the additional noise mentioned in Section II. Finally, Section IV discusses how we obtain the required SWPF rejection ratio in WDM systems.

II. Additional Noise due to OTDR Light

Fig. 2 shows one example of a measured OTDR pulse spectrum with a width of 100 ns received at an ONU. Since OTDR light is a train of pulses with a quasirectangular shape, lobes are formed at periods of the reciprocal of the pulsewidth. When the sidelobes are superimposed on the subcarriers in the frequency domain as shown in this figure, the video quality of the SCM signals is degraded.

The extra noise $n_{\mathrm{OTDR}}(t)$ at an ONU depends on the fundamental OTDR pulse waveform $n_{\mathrm{pulse}}(t)$ and intensity fluctuation noise $n_f(t)$ as shown in the following equation:

$$n_{\mathrm{OTDR}}(t) = (1 + n_f(t)) \cdot n_{\mathrm{pulse}}(t). \quad (1)$$

Manuscript received April 23, 1999; revised October 20, 1999.

The authors are with NTT Access Network Service Systems Laboratories, Ibaraki 305-0805, Japan (e-mail: yamamoto@ansl.ntt.co.jp).

Publisher Item Identifier S 0733-8724(00)02192-7.

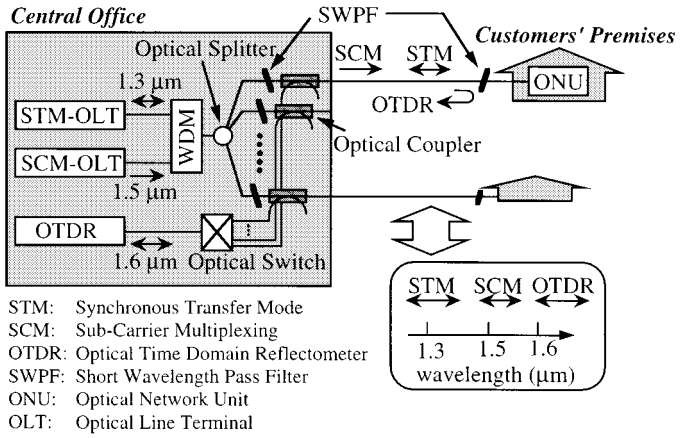

Fig. 1. Schematic illustration of an in-service measurement system in a WDM system in which synchronous transfer mode (STM) and subcarrier multiplexing (SCM) signals are propagated in an optical fiber.

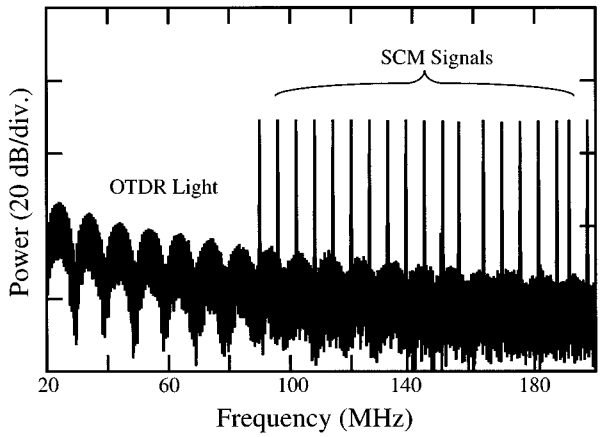

Fig. 2. Experimentally observed spectrum of OTDR light with a pulsewidth of 100 ns and SCM signals.

There are two types of fluctuation noise. One is intrinsic intensity noise caused by the intensity fluctuation of the OTDR light source [11]. The other is mode partition noise induced by the OTDR light propagation in an optical fiber [12]. These two types of noise are sufficiently large to make the effect of the shot noise caused by the OTDR light to become negligible.

A. Fundamental Pulse-Induced Noise

Fig. 3 shows an example of a video image affected by OTDR light. The noise appears as pairs of white lines. The distance between the two lines of the pair corresponds to the OTDR pulsewidth on each scanning line of the monitor. Moreover, these pairs of lines repeat at the pulse repetition rate. Therefore, we must obtain the temporal response function of the pulse train from a bandpass filter (BPF) with one subcarrier frequency band. Since the OTDR pulse is a periodic signal, the response function $n^1_{\text{pulse}}(t)$ can be given by the following equation with the transfer function $H(f)$ of the BPF

$$n^1_{\text{pulse}}(t) = \sum_{n=-\infty}^{\infty} c_n \cdot H(nf_0) \cdot e^{j2\pi(nf_0 t)} \tag{2}$$

where c_n is the expansion coefficients of complex Fourier series and f_0 is the reciprocal of the OTDR pulse repetition cycle T.

When we express the OTDR pulse, $n^0_{\text{pulse}}(t)$, as the sum of the repeated solitary pulses:

$$n^0_{\text{pulse}}(t) = \sum_{n=-\infty}^{\infty} f_{\text{pulse}}(t - nT) \tag{3}$$

c_n can be expressed as the following equation:

$$c_n = \frac{1}{T} \cdot F_{\text{pulse}}(nf_0) \tag{4}$$

where $F_{\text{pulse}}(f)$ is the Fourier transform of $f_{\text{pulse}}(t)$. If the OTDR pulse waveform is rectangular with a pulsewidth τ, $f_{\text{pulse}}(t)$ is given by

$$f_{\text{pulse}}(t) = \begin{cases} 1 & (-\tau/2 \le t \le \tau/2) \\ 0 & (\text{otherwise}) \end{cases} \tag{5}$$

and thus $F_{\text{pulse}}(f)$ becomes

$$F_{\text{pulse}}(f) = \tau \cdot \frac{\sin(\pi f \tau)}{(\pi f \tau)}. \tag{6}$$

The transfer function $H(f)$ of the BPF is assumed to be

$$H(f) = \begin{cases} e^{-j2\pi f t_0} & (f_c \le |f| \le f_c + B_W) \\ 0 & (\text{otherwise}) \end{cases} \tag{7}$$

where t_0 is the group delay time of the BPF, f_c is the subcarrier frequency and B_W is the bandwidth of the BPF. Combining (2), (4), (6), and (7), the response function of an OTDR pulse in one subcarrier band becomes

$$n^1_{\text{pulse}}(t) = \sum_{n=n_1}^{n_2} 2 \cdot \left[\frac{\tau}{T} \cdot \frac{\sin(\pi n f_0 \tau)}{\pi n f_0 \tau}\right] \cdot \cos(2\pi n f_0 (t - t_0)) \tag{8}$$

where integers n_1 and n_2 are the closest to the transmittable start and stop frequencies of the BPF, respectively;

$$n_1 = f_c/f_0 + \varepsilon_1, \quad n_2 = (f_c + B_W)/f_0 + \varepsilon_2, \quad |\varepsilon_{1,2}| < 1/2. \tag{9}$$

Fig. 4 shows the calculated and measured output waveforms from the BPF. In the calculated waveform, the output response occurs before the pulse is input. This is because the amplitude and phase characteristics of the BPF are assumed to be ideal as shown in (7), and this assumption does not consider the causality. However, there is very good quantitative agreement between the measured and calculated peak values. To estimate the allowable received OTDR light power, we must suppose the worst case of OTDR light degradation. Namely, we have to calculate the peak power, and (8) is very effective for estimating the fundamental noise.

Since n^1_{pulse} indicates as the sum of the cosine waves in (8), the fundamental noise power P_{pulse} in a subcarrier signal band can be defined as

$$P_{\text{pulse}} = \frac{1}{2}\left(\max \cdot \left[\left|n^1_{\text{pulse}}(t)\right|\right]\right)^2 \cdot (\rho P_{\text{peak}})^2 R_D G \tag{10}$$

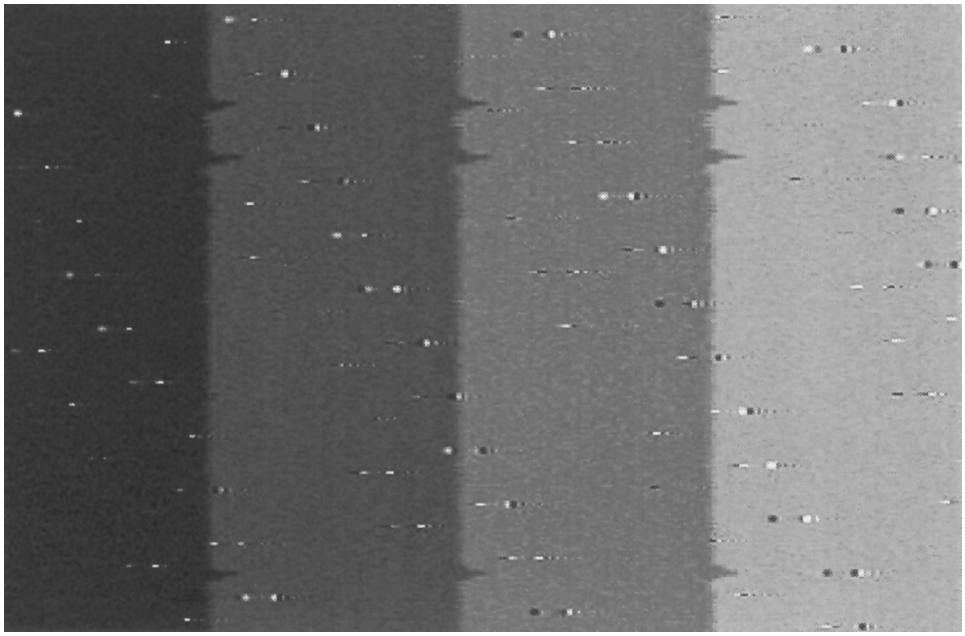

Fig. 3. Example of video image in which there is OTDR pulse induced noise. The pulsewidth and repetition cycle are 1 and 100 μs, respectively.

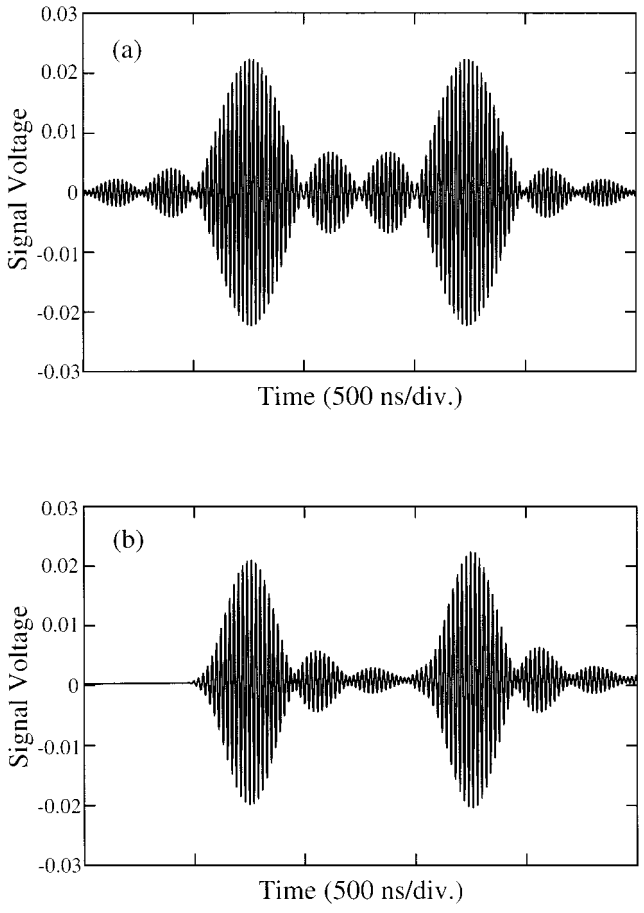

Fig. 4. (a) Calculated and (b) experimentally observed shapes of 1-μs OTDR pulse at the output of a bandpass filter with $f_c = 50$ MHz and $B_W = 4.2$ MHz. In the calculation, the BPF transmittance is assumed to be 0.9 which is the same as the measured value.

where ρ is the responsivity of the photodiode in an ONU, P_{peak} is the optical received peak power of the OTDR light at the ONU, R_D is the input resistance of the ONU, and G is the electrical power gain of the ONU.

1) Noise Dependence on Duty Ratio of OTDR Pulse: Fig. 5(a) and (b) shows the observed P_{pulse} data at $f_c = 50$ MHz in an experiment where OTDR light propagated through a few meters of optical fiber when the pulsewidth and repetition cycle were varied, alternately. This figure also shows the theoretical prediction we obtained from (10) using the experimental conditions. The numerical results are in excellent agreement with the observed data. Therefore, (10) is very useful for representing the dependence of the fundamental noise power on the duty ratio. Even though the pulse repetition rate was varied, the noise power remained constant as shown in Fig. 5(b). However, the power depends on the pulsewidth in Fig. 5(a). For example, the noise increased more than 5 dB when the width was broadened from 0.1 to 1 μs. These results show that we must take particular note of the pulsewidth when we estimate the allowable received OTDR light power.

2) Noise Dependence on Channel Frequency: Fig. 6 shows calculated and measured results of the fundamental noise power as a function of the channel frequency. The theoretical data shown by the thin solid line were obtained from (10). At frequencies above 50 MHz, the difference between the theoretical and experimental results increases with the frequency. This can be understood by noting that the actual pulse waveform deviates from an ideal rectangle because of the longer rise and fall times of the directly modulated OTDR light source. If the actual data are used as the solitary pulse waveform as shown in Fig. 7, the calculated results will agree with the measured ones. The solid line in Fig. 6 was obtained by using the above procedures, and it represents the quantitative behavior of the noise power very well as we expected. When evaluating the noise power in the higher frequency region, it is necessary to include the effect of the response properties of the OTDR light sources.

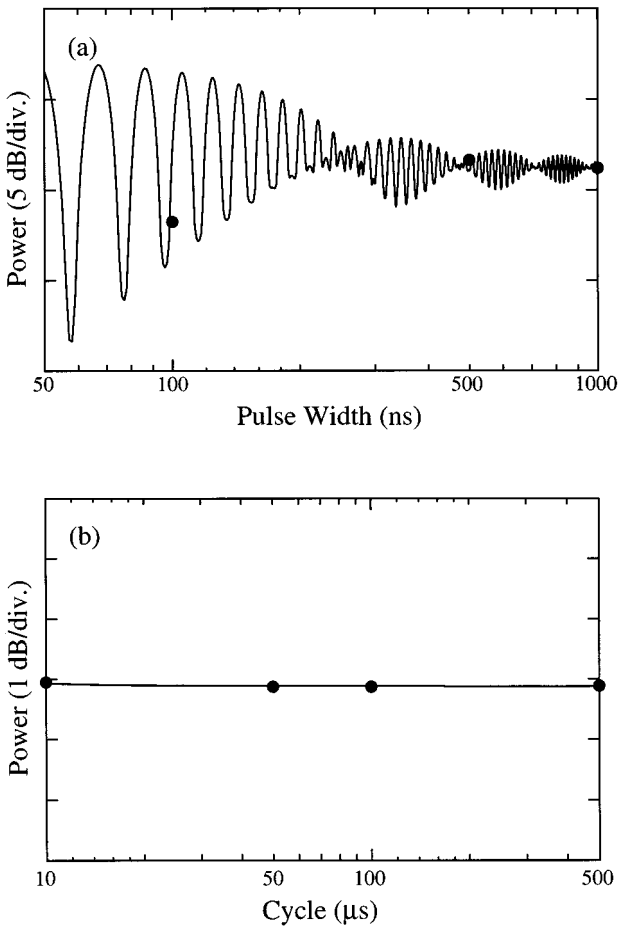

Fig. 5. Fundamental noise power $P_{\rm pulsc}$ as a function of the duty ratio of the OTDR pulse through the BPF with $f_c = 50$ MHz and $B_W = 4.2$ MHz. In (a), the pulsewidth is varied when the repetition rate has a constant value of 100 μs. By contrast, the repetition rate is varied at $\tau = 1$ μs in (b). The solid line and symbols show the theoretical and experimental data, respectively.

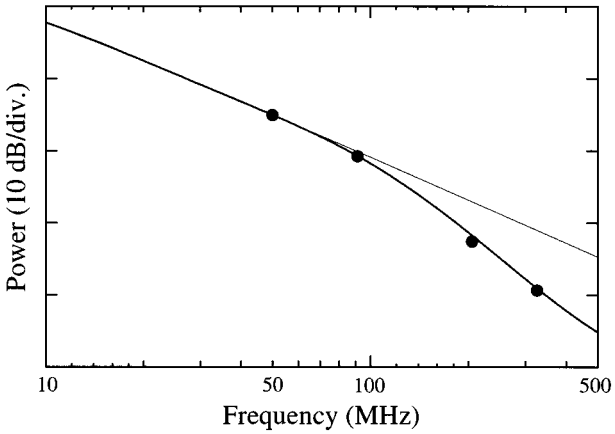

Fig. 6. Fundamental pulse-induced noise power $P_{\rm pulsc}$ as a function of frequency. Symbols show the measured power when 1-μs OTDR pulses propagate through a BPF with $B_W = 4.2$ MHz. The thin and bold solid lines show the calculated power for ideal rectangular and actual pulse waveforms, respectively.

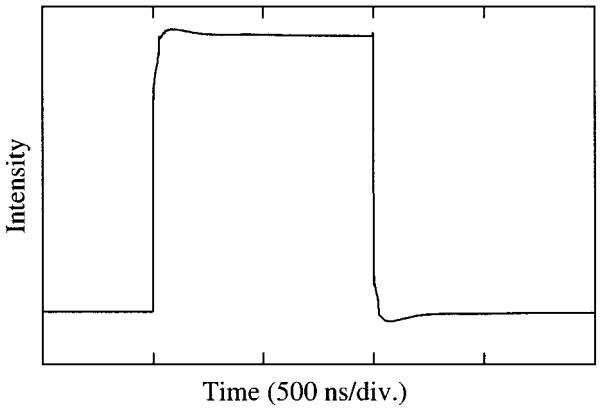

Fig. 7. OTDR pulse waveform emitted from the FP-LD used in the experiments. The form is quasirectangular.

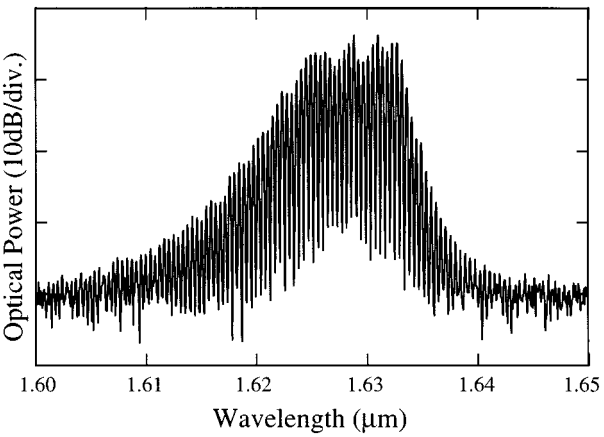

Fig. 8. Average optical spectrum of the FP-LD employed in the experiments. The FP-LD is directly modulated into pulse trains with a pulsewidth of 1 μs and a repetition rate of 100 μs. The center wavelength is 1.629 μm, the mode spacing is 0.4 nm, and the full-width at half-maximum (FWHM) is 8.2 nm.

B. Intensity Fluctuation Noise

Intrinsic intensity noise arises in a laser as a result of instantaneous optical power fluctuations in the laser. In addition, mode partition noise occurs due to fiber chromatic dispersion if multi longitudinal modes are emitted from the light source and the light propagates into the fiber. Since a Fabry–Perot laser diode (FP-LD) can easily provide high output powers, it is commonly used as an OTDR light source. The FP-LD has many longitudinal modes as shown in Fig. 8, and the distribution of power among the different longitudinal modes fluctuates randomly even when the total emitted power is constant. Moreover, optical access networks are commonly composed of 1.3-μm zero-dispersion single-mode (SM) fibers and the typical dispersion value of SM fibers is 24 ps/nm/km at the wavelengths in the 1.6-μm band.

Fig. 9 shows the measured intensity fluctuation noises for the OTDR light source with the spectrum shown in Fig. 8. The relative intensity noise (RIN) of the FP-LD decreases with an increase in frequency because it is well below the relaxation oscillation frequency of the laser [13]. Since the amplitude of the mode partition noise depends on the total dispersion of the propagated fiber [14], the RIN in the 10-km SM fiber is larger than that in the 2-km fiber. The extra noise due to the intensity fluctuation of the OTDR light, $n_{\rm RIN}(t)$, corresponds to the second term in (1) and is given by

$$n_{\rm RIN}(t) = n_f(t) \cdot n_{\rm pulse}(t). \tag{11}$$

Since the intensity fluctuation noise does not correlate with the fundamental OTDR pulse waveform, the power spectrum $P^0_{\rm RIN}(f)$ of the additional noise $n_{\rm RIN}(t)$ is given by

$$P^0_{\rm RIN}(f) = (\rho \cdot P_{\rm peak})^2 R_D G \times \sum_{n=-\infty}^{\infty} |c_n|^2 N_f(f - n \cdot f_0) \quad (12)$$

with $N_f(f)$ given by

$$N_f(f) = {\rm RIN}_1(f) + {\rm RIN}_2(f) \quad (13)$$

where ${\rm RIN}_1$ and ${\rm RIN}_2$ are the RIN of the light source and mode partition noise, respectively. When the transmission characteristics of the BPF is ideal as shown in (7), the intensity fluctuation noise power $P_{\rm RIN}$ in a subcarrier signal band becomes

$$P_{\rm RIN} = \int_{-\infty}^{\infty} |H(f)|^2 \cdot P^0_{\rm RIN}(f)\, df = (\rho \cdot P_{\rm peak})^2 R_D G \times \sum_{k=1}^{2} \sum_{i=n_1}^{n_2} \sum_{n=-\infty}^{\infty} |c_n|^2 {\rm RIN}_k((i-n) \cdot f_0). \quad (14)$$

Fig. 10(a) and (b) shows calculated results for the pulsewidth and repetition rate, respectively. The noise power increases with the pulse duty ratio. These calculated results accurately predicted the experimental observations.

In practice, OTDR light power is largely concentrated within a band of less than the frequency of B_W, and the power decreases as a function of frequency. Moreover, ${\rm RIN}_k$ gradually varies with frequency as shown in Fig. 9. Therefore, $|c_n|^2{\rm RIN}_k$ can be treated as zero when $|n| > B_W/f_0$, and (14) is given by a remarkably simple expression

$$P_{\rm RIN} = (\rho \cdot P_{\rm peak})^2 R_D G \sum_{k=1}^{2} \frac{\tau}{T} {\rm RIN}_k(f_c) \cdot B_W \quad (15)$$

where ${\rm RIN}_k$ is assumed to be constant within the signal band.

C. Total Noise Power Characteristics

From (1), the total noise power $P_{\rm OTDR}$, which is caused by the presence of OTDR light at an ONU, is given by

$$P_{\rm OTDR} = P_{\rm pulse} + P_{\rm RIN}. \quad (16)$$

Fig. 11 shows the frequency characteristic of the additional noise power obtained from (16) when an OTDR light with a pulsewidth of 1 μs and a pulse repetition cycle of 100 μs propagates through a 10-km single-mode fiber. In this calculation, the $P_{\rm pulse}$ values are obtained from the data shown with the bold solid line in Fig. 6, and $P_{\rm RIN}$ is estimated from (15) using the RIN measurement results shown in Fig. 9. The fundamental noise power dominates the total noise power. An interesting property is that the total noise power decreases with frequency in this figure, and thus the allowable received OTDR light power depends on the frequencies of the subcarriers allocated in lightwave SCM systems.

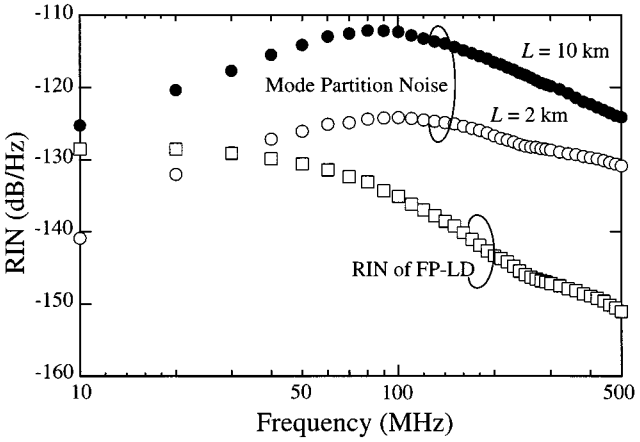

Fig. 9. Experimentally observed behavior of intrinsic relative intensity noise (squares) and mode partition noise at the output of a 2-km long SM fiber (open circles) and a 10-km long SM fiber (solid circles) for the FP-LD. The light from the FP-LD is a continuous wave.

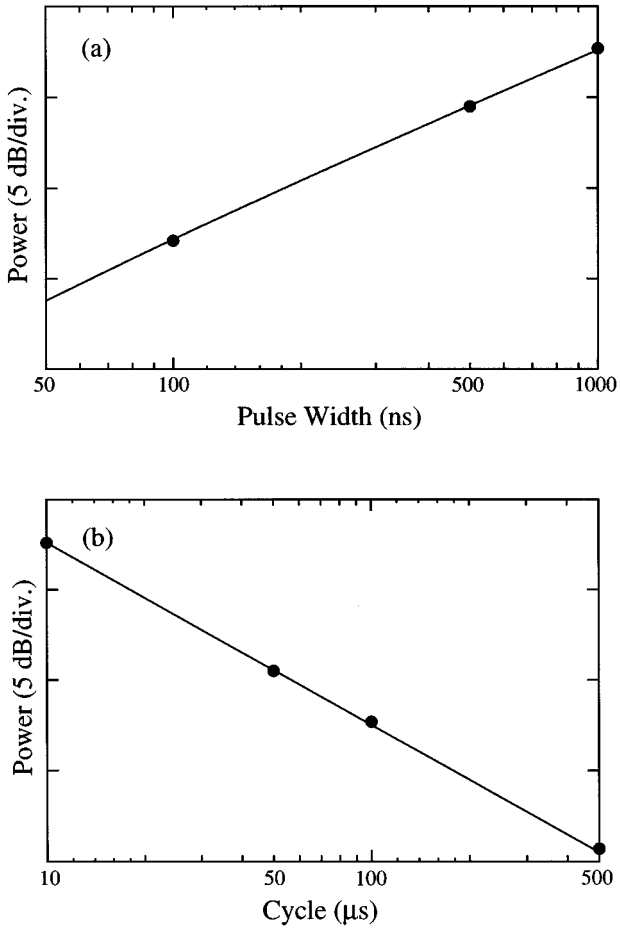

Fig. 10. Intensity fluctuation noise power $P_{\rm RIN}$ as a function of the duty ratio of an OTDR pulse when the pulse propagates through a BPF with $f_c = 50$ MHz and $B_W = 4.2$ MHz. (a) shows the dependence on the pulsewidth when the repetition rate is 100 μs. By contrast, (b) shows the dependence on the repetition cycle at $\tau = 1$ μs. The solid line and symbols show the theoretical and experimental data, respectively.

III. CNR Performance in Presence of OTDR Light

In this section, we describe the characteristics of CNR affected by the OTDR light contribution which we observed

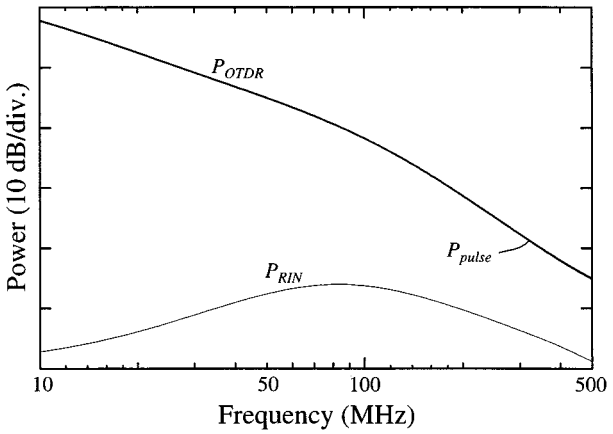

Fig. 11. Dependence of the additional noise power on frequency for a 10-km long SM fiber. The OTDR light from the FP-LD has a 1-μs pulsewidth and a 100-μs pulse repetition cycle, and it propagates through the BPF with B_W = 4.2 MHz.

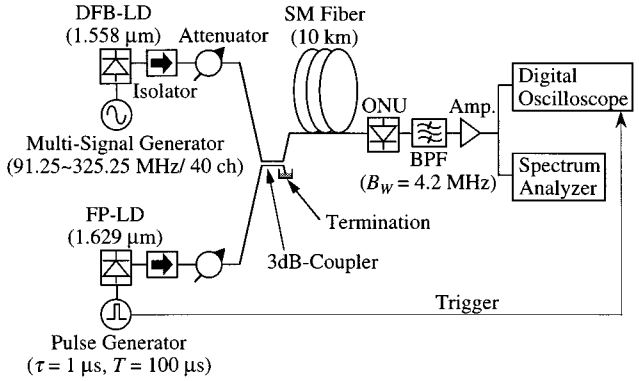

Fig. 12. Experimental setup used to observe the dependence of CNR on the received OTDR light power at an ONU.

experimentally for a 40-channel lightwave SCM system. Moreover, we clarify the way to estimate the allowable received OTDR light power by using previous noise analysis.

A. Experimental Setup for CNR Measurements

Fig. 12 shows the experimental setup. 40 subcarriers with frequencies from 91.25 to 325.25 MHz directly modulate the DFB-LD with a center wavelength of 1.558 μm. An optical carrier from the DFB-LD was propagated through a 10-km SM fiber and entered an ONU. The average received optical power was always kept at -8 dBm. By contrast, OTDR light with a pulsewidth of 1 μs and a repetition rate of 100 μs were obtained by directly modulating the FP-LD with the spectrum shown in Fig. 8. The OTDR pulse waveform was quasirectangular as shown in Fig. 7, and its center wavelength was 1.629 μm. The OTDR light was launched into the SM fiber via a 3-dB coupler and was received at the ONU. The received pulse was analyzed after it had propagated through a BPF with a bandwidth of 4.2 MHz. We measured the fundamental pulse-induced noise and intensity noise resulting from its instantaneous power fluctuation with a digital oscilloscope and a spectrum analyzer, respectively. We measured the CNR of the subcarriers at the ONU while varying the received peak OTDR light power from -35 to -15 dBm with an optical attenuator located in the front of the light source. The measurement subcarrier frequencies were 91.25 MHz (first channel) and 325.25 MHz (last channel). In the absence of the OTDR light, the CNR values were 44.2 and 44.5 dB at the first and last channel, respectively. If reflected light enters a light source, the intensity noise [15] and nonlinear distortion [16] become worse. Therefore, an optical isolator with an isolation of more than 50 dB was installed into the output port of each light source.

B. Experimental Results

The measured CNR as a function of the received peak power of the OTDR light is shown with filled circles in Fig. 13. In both channels, the CNR decreased with the received peak power. Moreover, the degree of its reduction at 91.25 MHz was more emphatic than that at 325.25 MHz because the total noise power decreased with an increase in the channel frequency as shown in Fig. 11. Therefore, if one channel with the lowest subcarrier frequency satisfies the required CNR, the service quality of all the channels is maintained even though the OTDR light enters the ONU.

Moreover, we considered whether or not the OTDR light affects the signal distortion. This is because pump depletion occurs if the power transmitted through an optical fiber exceeds the Brillouin threshold which is relatively low. However, neither the composite second-order (CSO) nor the composite triple-beat (CTB) increased even though an OTDR pulse with a peak power of 0 dBm propagated in the fiber, and these values were always less than -70 dBc and -66 dBc, respectively. The Brillouin threshold depends on the linewidth of the signal light source and fiber length. However, the linewidth of the directly modulated light source was more than 100 MHz which was wider than that of Brillouin-gain profile. Moreover, the fiber length was 10 km which was relatively short. As a result, the threshold became more than 10 dBm and the OTDR light did not increase the signal distortion.

We observed the video images of the first channel on a monitor when the CNR had fallen by 20 and 1 dB because of OTDR light injection into the ONU. When decreased by 20 dB, the white lines induced by the OTDR light appear on the monitor as shown in Fig. 3. However, the noise can be eliminated by limiting the CNR degradation to 1 dB.

C. Analysis of CNR

In the presence of OTDR light at an ONU, CNR is given by

$$\mathrm{CNR}^{-1} = \mathrm{CNR}_0^{-1} + P_{\mathrm{OTDR}}/P_s \tag{17}$$

where CNR_0 is the value when the OTDR light is excluded, and P_s is the average received subcarrier signal power. P_s is written as in Ref. [17]

$$P_s = \frac{1}{2}(m \cdot \rho P_{\mathrm{ls}})^2 R_D G \tag{18}$$

where m is the optical intensity modulation index per channel and P_{ls} is the average received signal light power at the ONU.

Fig. 13 shows CNR estimated from (17) under conditions identical to those for the measurements shown in Tables I and II. The solid curve shows the calculated CNR as a function of the received peak power of the OTDR light when the additional

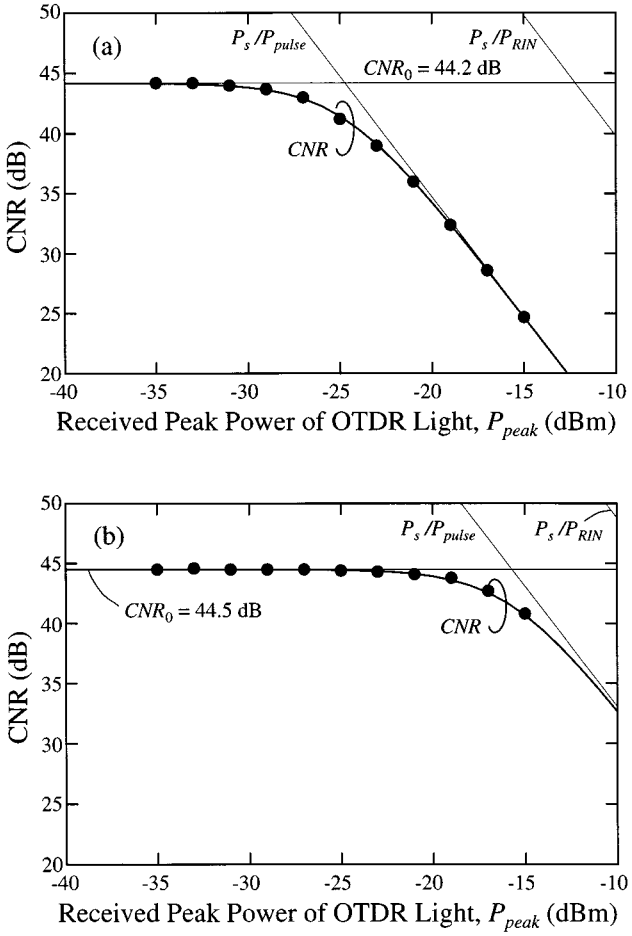

Fig. 13. Variation of the CNR with the received peak OTDR light power from the FP-LD at the first and last channels corresponding to (a) $f_c = 91.25$ MHz and (b) 325.25 MHz, respectively. The circles show the measured CNR and the solid curve corresponds to the theoretical results obtained from (17).

noise power is given by the data shown in Fig. 11. Moreover, the CNR limitation due to each additional noise is shown with the light solid line. Both the calculated and measured results obey the P_{peak}^2 dependence on the received peak power, and (17) is able to show the quantitative features of the CNR degradation for the received power. Therefore, (17) is very important for estimating the allowable received power. When the tolerance Δd for the CNR decrease is defined by

$$\Delta d = \text{CNR}/\text{CNR}_0 \tag{19}$$

the allowable received peak power P_{allow} of the OTDR light is obtained from (17) as follows:

$$P_{\text{allow}}^2 = \frac{1-\Delta d}{\Delta d} \cdot \frac{S_{\text{subcarrier}}}{N_{\text{OTDR}}} \cdot \text{CNR}_0^{-1} \tag{20}$$

where

$$N_{\text{OTDR}} = \frac{1}{2}\left(\max \cdot \left[\left|n_{\text{pulse}}^1(t)\right|\right]\right)^2 + \sum_{k=1}^{2} \frac{\tau}{T}\text{RIN}_k(f_c) \cdot B_W \tag{21}$$

and

$$S_{\text{subcarrier}} = \frac{1}{2}(mP_{\text{ls}})^2. \tag{22}$$

When $\Delta d = -1$ dB which corresponds to the video quality without OTDR noise in the image, and P_{allow} is estimated to be -28 dBm from (20). It should be noted that (20) shows that the allowable power is independent of the modulation index m because CNR_0 is proportional to m^2. Therefore, P_{allow} does not change for a constant value of Δd as long as the variation of CNR_0 is caused by the change of m. However, P_{allow} increases when CNR_0 increases with P_{ls}.

IV. Required SWPF Rejection Ratio

NTT has developed WDM systems which can simultaneously transmit both STM and SCM signals over one fiber. To measure an in-service fiber by employing an OTDR in the WDM system, as shown in Fig. 1, the OTDR light wavelength must not be in a signal band, and an SWPF is installed into an ONU input port to reject the OTDR light. In this section, we estimate the required rejection ratio of the SWPF by using (20) in the WDM system.

Fig. 14 is a schematic illustration of an ONU for the WDM system [18]. The STM and SCM signals from the central office are divided into each port by a WDM filter. A little OTDR light enters the ONU through the SWPF since it does not have a 100% rejection ratio. The OTDR light is also divided into two ports by the WDM filter. Because the wavelength of the OTDR light is longer than that of the STM signal, a large quantity of light is transmitted to the SCM port. The OTDR pulse peak power at the input port of the photodiode (PD) of the SCM signal, $P_{\text{PD}}(\text{SCM})$, is given by the following equation with the crosstalk ratio C of the WDM filter at the pulse wavelength

$$P_{\text{PD}}(\text{SCM}) = R(1-C) \cdot P_{\text{SWPF}} \tag{23}$$

where R is the SWPF rejection ratio, and P_{SWPF} is the pulse peak power at the SWPF input port. When we carry out in-service measurements, $P_{\text{PD}}(\text{SCM})$ must be less than the allowable received pulse power which can be obtained from (20). Therefore, the rejection ratio required to maintain the SCM signal quality, $R(\text{SCM})$, is given by

$$R(\text{SCM}) \le \frac{1}{1-C} \cdot \frac{P_{\text{allow}}}{P_{\text{SWPF}}} \tag{24}$$

where P_{allow} is the allowable OTDR pulse peak power at the PD.

By contrast, the OTDR pulse peak power $P_{\text{PD}}(\text{STM})$ at the input port of a PD receiving an STM signal is given by

$$P_{\text{PD}}(\text{STM}) = \frac{3}{4}RC \cdot P_{\text{SWPF}} \tag{25}$$

where the coupling ratio of the LD port side in an asymmetric Y-splitter is assumed to be 75% [18]. In [10], $P_{\text{PD}}(\text{STM})$ for narrowband ISDN services is limited by

$$P_{\text{PD}}(\text{STM})/P_{\text{ls}}(\text{STM}) \le 10^{-15/10} \tag{26}$$

where $P_{\text{ls}}(\text{STM})$ is the received average power of the STM signal at the PD for the STM. Combining (25) and (26), we obtain the required rejection ratio for the STM signal, $R(\text{STM})$, as the following equation:

$$R(\text{STM}) \le \frac{(4/3) \cdot 10^{-15/10}}{C} \cdot \frac{P_{\text{ls}}(\text{STM})}{P_{\text{SWPF}}}. \tag{27}$$

TABLE I
EXPERIMENTAL CONDITIONS FOR LIGHTWAVE SCM SYSTEM

Subcarrier Frequencies	91.25 ~ 325.25 MHz
Number of Channels	40
Light Source	DFB-LD
Center Wavelength	1.558 μm
Optical Modulation Index per Channel (m)	0.045
Transmission Line	10-km SM Fiber
Average Optical Received Power at ONU (P_{ls})	-8 dBm
CNR in absence of OTDR light (CNR_0)	44.2 dB (91.25 MHz) 44.5 dB (325.25 MHz)
Signal Bandwidth (B_W)	4.2 MHz

TABLE II
EXPERIMENTAL CONDITIONS FOR OTDR

Light Source	FP-LD
Center Wavelength	1.629 μm
RIN of Light Source (RIN_1)	-134 dB/Hz* -147 dB/Hz**
RIN of Mode Partition Noise (RIN_2)	-112 dB/Hz* -121 dB/Hz**
Pulse Width (τ)	1 μs
Pulse Repetition Cycle (T)	100 μs
Optical Received Peak Power at ONU (P_{peak})	-35 ~ -15 dBm

* at 91.25 MHz, ** at 325.25 MHz

In a WDM system, the required rejection ratio can be obtained by combining (24) and (27). Fig. 15 shows this rejection ratio including the parameters shown in Tables I and II. In this analysis, P_{SWPF} and $P_{\mathrm{ls}}(\mathrm{STM})$ were 0 and -37 dBm, respectively. Moreover, the CNR degradation tolerance was assumed to be 1 dB, so we set P_{allow} at -28 dBm as mentioned in the previous section. If the rejection ratio is less than that shown by the solid line in Fig. 15, in-service measurement can be carried out employing the OTDR. The most noteworthy feature of Fig. 15 is that the required rejection ratio, whose value is -28 dB, is independent of the crosstalk ratio when $C < -23$ dB.

V. CONCLUSION

This paper proposed a technique for estimating the allowable received power of light from an OTDR at ONU's in optical transmission systems using SCM techniques. If the actual received power of the OTDR light is less than the allowable power, in-service measurement can be carried out because the CNR of all channels satisfies the required condition even though the OTDR light enters the ONU.

A detailed discussion showed that there were three significant additional types of noise induced by the OTDR light in one subcarrier frequency band: fundamental OTDR pulse-induced noise, the intrinsic intensity noise of the OTDR light source, and mode partition noise caused by OTDR light propagation in optical fibers. The intensity of these noises depends on the OTDR pulse waveform, the duty ratio of the pulse train, the pulse peak power at an ONU, the relative intensity noise of the OTDR light source, the light propagation length, and the subcarrier frequency.

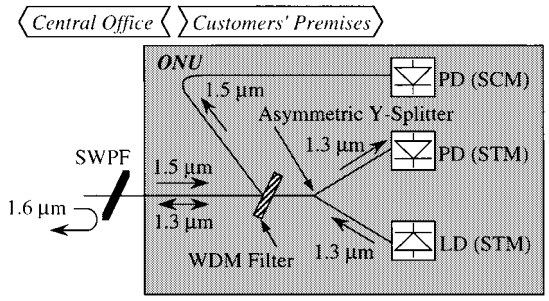

Fig. 14. Schematic illustration of an ONU used in a WDM system.

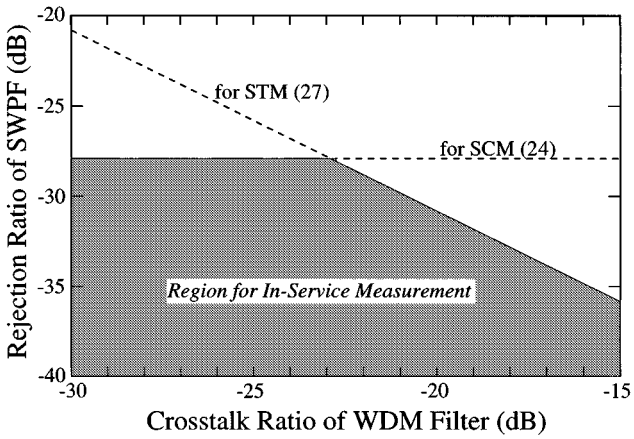

Fig. 15. Required SWPF rejection ratio as a function of crosstalk ratio of a WDM filter in the ONU.

From the discussion, we analyzed the quantitative behavior of the CNR degraded by OTDR light injection into an ONU, and also verified the accuracy of the estimate using measured results for a 40-channel lightwave SCM system with subcarrier frequencies from 91.25 to 325.25 MHz. An interesting property is that the service quality of all channels is ensured if the CNR in one specific channel with the lowest subcarrier frequency exceeds the required CNR in the presence of OTDR light.

When designing in-service measurement systems, CNR analysis is useful for estimating such important parameters as the required isolation for OTDR light in a SWPF which is installed in the front of ONU's. The required SWPF isolation can be calculated by using the estimation technique in a WDM system which provides STM and SCM signals. The calculation results showed the dependence of the SWPF isolation on the crosstalk ratio of a WDM filter installed in the ONU. By using the designed technique, we can carry out in-service testing on WDM systems.

REFERENCES

[1] R. Olshansky, V. A. Lanzisera, and P. M. Hill, "Subcarrier multiplexed lightwave systems for broad-band distribution," *J. Lightwave Technol.*, vol. 7, pp. 1329–1342, Sept. 1989.
[2] W. I. Way, "Subcarrier multiplexed lightwave system design considerations for subscriber loop applications," *J. Lightwave Technol.*, vol. 7, pp. 1806–1818, Nov. 1989.
[3] T. E. Darcie and G. E. Bodeep, "Lightwave subcarrier CATV transmission systems," *IEEE Trans. Microwave Theory Tech.*, vol. 38, pp. 524–533, May 1990.

[4] K. Kikushima, K. Suto, H. Nakamoto, H. Yoshinaga, C. Kishimoto, M. Kawabe, K. Kumozaki, and N. Shibata, "Super-wide-band optical FM modulation scheme and its application to multichannel AM video transmission systems," *IEEE Photon. Technol. Lett.*, vol. 8, pp. 839–841, June 1996.
[5] H. Dai, S. Ovadia, and C. Lin, "Hybrid AM-VSB/M-QAM multichannel video transmission over 120 km of standard single-mode fiber with cascaded erbium-doped fiber amplifiers," *IEEE Photon. Technol. Lett.*, vol. 8, pp. 1713–1715, Dec. 1996.
[6] E. Yoneda, K. Suto, K. Kikushima, and H. Yoshinaga, "All-fiber video distribution (AFVD) systems using SCM and EDFA techniques," *J. Lightwave Technol.*, vol. 11, pp. 128–137, Jan. 1993.
[7] B. Clesca, P. Bousselet, J. Auge, J. P. Blondel, and H. Fevrier, "1480-nm pumped erbium-doped fiber amplifiers with optimized noise performance for AM-VSB distribution systems," *IEEE Photon. Technol. Lett.*, vol. 6, pp. 1318–1320, Nov. 1994.
[8] T. E. Darcie, G. E. Bodeep, and A. A. M. Saleh, "Fiber-reflection-induced impairments in lightwave AM-VSB CATV systems," *J. Lightwave Technol.*, vol. 9, pp. 991–995, Aug. 1991.
[9] S. Furukawa, H. Suda, F. Yamamoto, Y. Koyamada, T. Kokubun, and I. Takahashi, "Optical fiber line test and management system for passive double star networks and WDM transmission systems," in *44th. IWCS Proc.*, 1995, pp. 640–648.
[10] N. Tomita, H. Takasugi, N. Atobe, I. Nakamura, F. Takaesu, and S. Takashima, "Design and performance of a novel automatic fiber line testing system with OTDR for optical subscriber loops," *J. Lightwave Technol.*, vol. 12, pp. 717–726, May 1994.
[11] K. Sato, "Intensity noise of semiconductor laser diodes in fiber optic analog video transmission," *IEEE J. Quantum Electron.*, vol. QE-19, pp. 1380–1391, Sept. 1983.
[12] K. Peterman and G. Arnold, "Noise and distortion characteristics of semiconductor lasers in optical fiber communication systems," *IEEE J. Quantum Electron.*, vol. QE-18, pp. 543–555, Apr. 1982.
[13] M. Yamada, "Theory of mode competition noise in semiconductor injection lasers," *IEEE J. Quantum Electron.*, vol. QE-22, pp. 1052–1059, July 1986.
[14] G. Grosskopf, L. Kuller, and E. Patzak, "Laser mode partition noise in optical wideband transmission links," *Electron. Lett.*, vol. 18, no. 12, pp. 493–494, 1982.
[15] O. Hirota, Y. Suematsu, and K. S. Kwok, "Properties of intensity noises of laser diodes due to reflected waves from single-mode optical fibers and its reduction," *IEEE J. Quantum Electron.*, vol. QE-17, pp. 1014–1020, June 1981.
[16] K. Kikushima and Y. Suematsu, "Nonlinear distortion properties of laser diode influenced by coherent reflected waves," *Trans. IEICE*, vol. E67, pp. 19–25, Jan. 1984.
[17] W. I. Way, R. S. Wolff, and M. Krain, "A 1.3-μm 35-km fiber-optic microwave multicarrier transmission system for satellite earth stations," *J. Lightwave Technol.*, vol. 5, pp. 1325–1332, Sept. 1987.
[18] N. Uchida, Y. Yamada, Y. Hibino, Y. Suzuki, and N. Ishihara, "Low-cost hybrid WDM module consisting of a spot-size converter integrated laser diode and a waveguide photodiode on a PLC platform for access network systems," *IEICE Trans. Electron.*, vol. E80-C, no. 1, pp. 88–97, Jan. 1997.

Fumihiko Yamamoto was born in Yamaguchi, Japan, on January 25, 1966. He received the B.E. and M.E. degrees in mechanical engineering from Kyusyu University, Fukuoka, Japan, in 1989 and 1991, respectively.

In 1991, he joined NTT Transmission Systems Laboratories, Ibaraki, Japan, where he has been engaged in research and development on in-service measurement technologies in optical access networks. He is now a Research Engineer of NTT Access Network Service Systems Laboratories, Ibaraki, Japan, where he works on WDM optical network design in metropolitan and local areas.

Mr. Yamamoto is a member of the Institute of Electronics, Information and Communication Engineers (IEICE) of Japan.

Tsuneo Horiguchi (M'87–SM'96) was born in Tokyo, Japan, on June 5, 1953. He received B.E. and Dr.Eng. degrees from the University of Tokyo, Tokyo, Japan, in 1976 and 1988, respectively.

In 1976, he joined the NTT Ibaraki Electrical Communication Laboratories, where he worked on the measurement of the transmission characteristics of optical fiber cable. Since 1988, he has worked in the field of optical fiber distributed sensing. He is presently the Executive Manager of the Advanced Transmission Media Project, NTT Access Network Service Systems Laboratories, Ibaraki, Japan.

Dr. Horiguchi is a member of the Institute of Electronics, Information and Communication Engineers (IEICE) of Japan, the Optical Society of Japan, and the Optical Society of America (OSA).